SCIENCE CHINA Materials ARTICLES

mater.scichina.com link.springer.com

Published online 12 October 2018 | https://doi.org/10.1007/s40843-018-9355-0

Sci China Mater 2019, 62(4): 519–526

An *in-situ* room temperature route to $CuBiI_4$ based bulk-heterojunction perovskite-like solar cells

Busheng Zhang[1,2], Yan Lei[1*], Ruijuan Qi[3], Haili Yu[1], Xiaogang Yang[1], Tuo Cai[1] and Zhi Zheng[1*]

ABSTRACT **Both bismuth and copper are non-toxic and earth-abundant elements suitable for lead-free halide perovskite-like photovoltaic devices. Here, we report a highly facile route for *in-situ* producing copper-bismuth-iodide ($CuBiI_4$) thin films directly on ITO substrate at room temperature, by utilizing a Bi-Cu alloy layer as precursor. X-ray diffraction and transmission electron microscopy (TEM) results verified the formation of well crystallized $CuBiI_4$ thin films with [222] orientation. The transient photovoltage (TPV) analysis revealed that the $CuBiI_4$ is an n-type semiconductor with a suitable band gap of ~1.81 eV, preferable to photoelectric conversion compared with $CH_3NH_3PbI_3$. It is very interesting that the subsequent spin-coating process of the classical Spiro-MeOTAD organic solution with TBP and acetonitrile resulted in a dense and smooth $CuBiI_4$:Spiro-MeOTAD bulk-heterojunction film. The preliminarily fabricated simple sandwich structures of ITO/$CuBiI_4$:Spiro-MeOTAD/Au hybrid solar cell devices displayed efficient photovoltaic performance with the PCE up to 1.119% of the best sample. The room temperature direct metal surface elemental reaction (DMSER) method may provide a new insight for all-inorganic lead free perovskite-like $A_aB_bX_x$ compounds and high performance photovoltaic devices.**

Keywords: copper-bismuth-iodide, $CuBiI_4$, room temperature, lead-free, perovskite-like, bulk-heterojunction, solar cells

INTRODUCTION

Although the organo-lead halide perovskites have gained tremendous progress during the past ten years [1–6], the concern about toxic lead elements pushed researchers to continuously seek and explore new lead-free compounds with perovskite or perovskite-like structures [7,8]. Theoretically, there are tens of metal element candidates, including transition metals, group-14 elements, alkaline-earth metals and even lanthanides [9], which can meet the demand of the homovalent or heterovalent substitution of lead, with isovalent cations and aliovalent metal cations [9]. Among these metal elements, Sn and Ge in the same family as lead and the related perovskite solar cells have been extensively studied, which exhibited the highest power conversion efficiency (PCE) of up to about 8% in the current lead-free perovskite photovoltaics [10–16]. However, the tin- and germanium-based perovskite devices still suffered from the severe unstability. Bismuth-based lead free organo-halide perovskites, such as $(CH_3NH_3)_3Bi_2I_9$ [17–22], $Cs_3Bi_2I_9$ [23–27], and Cs_2AgBiX_6 (X=Cl, Br, I) [28–31] have recently attracted more attention due to its non-toxic and earth abundant characteristics of bismuth element, although the corresponding PCE are still very low [26].

A promising analogue is the bismuth based all-inorganic perovskite-like/rudorffites $A_aB_bX_x$ compounds (A=Ag, Cu; B=Bi, Sb; X=I, Br and $x=a+3b$), such as the Ag-Bi-I (Ag_3BiI_6, Ag_2BiI_5, $AgBiI_4$, and Ag_2BiI_7) system [32]. The preparation of $AgBiI_4$ generally relies on the reaction of AgI and BiI_3 at high temperatures [32,33]. For example, Turkevych *et al.* [32] obtained a series of ternary Ag-Bi-I compounds at 600°C, and they assembled an effective FTO/c-m-TiO_2/Ag_3BiI_6/PTAA/Au solar cell device with an improved PCE of 4.3%, which further demonstrated the applicability of the proposed rudorffites $A_aB_bX_x$ structures. Considering both abundance and cost, the replacement of Ag with Cu element in $A_aB_bX_x$ system

[1] Key Laboratory for Micro-Nano Energy Storage and Conversion Materials of Henan Province, College of Advanced Materials and Energy, Institute of Surface Micro and Nano Materials, Xuchang University, Xuchang 461000, China
[2] School of Civil Engineering and Communication, North China University of Water Resources and Electric Power, Zhengzhou 450046, China
[3] Key Laboratory of Polar Materials and Devices, Ministry of Education, Department of Electronic Engineering, East China Normal University, Shanghai 200241, China
* Corresponding authors (emails: zzheng@xcu.edu.cn (Zheng Z); leiyan@xcu.edu.cn (Lei Y))

should be highly preferred. A_xBiI_4 (A=Ag, Cu) structures have been investigated as potential ionic conductors several decades ago and several recent papers [32,34] have predicted the potential application of copper-bismuth-iodide compound in photovoltaic similar to the $AgBiI_4$. However, we noticed that there are almost no reports of such a promising ternary compound, and even the exact crystal structures are still not clear. The only literature related to the $CuBiI_4$ crystal structure was published in 1991 by Fourcroy *et. al.* [35], which only gave the incomprehensive crystal structure data. Until very recently, Hayase *et. al.* [36] firstly developed a solution-processed low temperature route to synthesize (111) faceted $CuBiI_4$ crystals, assisted by high vapor pressure of tributyl phosphate and HI-DMA co-solvent, which needs to be completely removed before device assembling. Analogous to the previous reports of bismuth-based perovskite, CuI and BiI_3 powders are also required and the crystallization process is highly sensitive to precursor solution concentration. A wide band gap of 2.67 eV of the resulting copper-bismuth-iodide thin film with 0.82% PCE of the best sample was obtained.

Our group [37–41] has previously explored a direct metal surface elemental reaction (DMSER) method to fabricate various chalcogenide and iodide thin films for photovoltaics. However, the reaction between elemental bismuth and iodine was difficult because the elemental bismuth layer easily vaporizes even at low temperature. In this work, by taking advantage of the DMSER method with Bi-Cu alloy and elemental iodine as precursor, we *in-situ* fabricated $CuBiI_4$ thin films on ITO at room temperature. A gray black thin film was finally presented with a suitable band gap of ~1.81 eV for solar harvesting and photovoltaics. By using the newly obtained $CuBiI_4$ semiconductor layer, we next fabricated a series of very simple ITO/$CuBiI_4$:Spiro-MeOTAD/Au bulk-junction solar cell devices which exhibited efficient photovoltaic performance, although there is only a hybrid layer between the two electrodes. This Bi-Cu alloy initiated fabrication of copper-bismuth-iodide thin films as well as the construction of the bulk-heterojunction solar cell devices may exploit a new purpose of the DMSER method for future $A_aB_bX_x$ photovoltaics.

EXPERIMENTAL SECTION

Materials

All materials were commercially available and used without further purification. The Bi-Cu alloy target (Beijing Gao Dewei Metal Company, China) with mole ratio of 1:1 was used for preparing elemental thin film precursor. Elemental I_2 grains (Alfa Aesar) with purity of 99% were used for fabricating $CuBiI_4$.

Preparation of Bi-Cu alloy thin films on ITO substrates

ITO substrates (10 Ω/square, South China Sci. & Tech. Com. Ltd.) were ultrasonically washed with deionized water, detergent and deionized water in sequence. Then, these ITO substrates were treated with a mixture of $NH_3{\cdot}H_2O$:H_2O_2:H_2O (1:2:5, *v*/*v*) at 80°C for about 30 min. After blow-drying with nitrogen, the ITO substrates were treated with UV-O_3 (NOVASCAN PSD UV4, USA) for 15 min for further use. The Bi-Cu alloy thin films were deposited on the clean ITO substrate by magnetron sputtering (EXITECH K575X, UK) with a pressure of 8×10^{-3} mbar and current of 40 mA under Ar atmosphere. A film thickness monitor (FTM) was used for determining the thickness of films.

$CuBiI_4$ thin films fabrication

About 1 g of I_2 and Bi-Cu alloy thin films were sealed in a container in glove box (N_2 gas filled), avoiding direct contact of I_2 particles and Bi-Cu alloy thin films. After the reaction of I_2 vapor with Bi-Cu alloy at room temperature for 10 h, a gray black $CuBiI_4$ thin film can be obtained on the ITO substrate.

Solar cell device fabrication

The prepared $CuBiI_4$ thin films were used to assemble solar cell devices without any further treatment. Firstly, 80 mg 2,2',7,7'-tetrakis-(*N*,*N*-di-*p*-methoxyphenyl-amine)-9,9'-spirobifluorene (Spiro-MeOTAD, Sigma-Aldrich), 27.5 μL 4-*tert*-butyl pyridine (Aladdin) and 17.5 μL lithium bis(trifluoromethanesulfonyl)imide (Li-TFSI) solution (520 mg Li-TSFI in 1 mL acetonitrile (Aladdin, 99.8%)) were dissolved in 1 mL of chlorobenzene (Aladdin, 99.8%) to prepare a Spiro-MeOTAD chlorobenzene solution; secondly, the prepared $CuBiI_4$ thin films were coated with the Spiro-MeOTAD mixed organic solvent solution by spin-coating method with 3,000 rpm in glove box; finally, about 80 nm Au electrode was coated by thermal evaporation method (EMITCH K950X, UK) to complete the solar cell devices assembling. The active areas of the resulting solar cell devices are 0.15 cm^2.

Characterization

The X-ray diffraction patterns of the samples were collected in the range of 10°–90°, with an increasement of 0.02 degree and a step of 0.1 second. The X-ray was generated by a Cu target X-ray tube with 40 mA current

and 40 kV voltage. The morphology of the samples was monitored by scanning electron microscopy (SEM, Hitachi S-4800) and atomic force microscopy (AFM, Dimension Icon, Bruker). TEM observations were performed on a transmission electron microscope (JEOL, JEM-2100F) with 200 kV voltage. The light absorption character of the samples was evaluated with a UV-Vis-NIR spectrophotometer (Agilent, Carry 5000). The transient surface photovoltage (TPV) data of the thin films were recorded by using a digital TDS oscilloscope (500MHz, TDS 3054C, Tektronix), and the excited light was a Nd:YAG pulsed laser (355 nm, 4 ns, Quantel Brilliant Eazy, BRILEZ/IR-10). The valance band (VB) of the samples were measured by UPS setup equipped with a monochromatic He I source (21.2 eV) and a VG Scienta R4000 analyzer. $J-V$ curves of the solar cell devices were obtained by a Keithley 2440 source meter. The light was generated by a solar simulator (model 91192STS, Newport) equipped with an AM 1.5G filter, and the light intensity was 0.69 suns that was calibrated by a standard silicon reference meter (model 91150V, Newport). A commercial IPCE measurement system (66902 Arc Lamp, Newport) was used to test the external quantum efficiency of the solar cell devices.

RESULTS AND DISCUSSION

To fabricate the perovskite copper bismuth iodide ternary compound, the Bi-Cu alloy thin films with certain thickness were firstly deposited by magnetron sputtering on the ITO substrate, and then reacted with elemental I_2 at room temperature (RT), and then, a large area uniform gray black copper bismuth iodide can be obtained. A schematic diagram of the manufacture progress is shown in Fig. 1. The reaction mechanism was also assumed according to the experimental results. Considering that the pure bismuth layer could not react with iodine at room temperature even after long term reservation in iodine atmosphere according to our experiments, we proposed that the formation of the copper bismuth iodide may be activated by the newly formed CuI ($2Cu+I_2 \rightarrow 2CuI$ (1)) in the first step, then the CuI reacted with Bi in the I_2 atmosphere to generate $CuBiI_4$ ($2CuI+2Bi+3I_2 \rightarrow 2CuBiI_4$ (2)). Keeping the elemental iodine overdosage in the current reaction is the key to fabricate pure $CuBiI_4$. Detailed experiments and reaction mechanism are beyond the scope of the current work and will be discussed in the future. We also found that the reaction between I_2 and layered Bi/Cu (mole ratio, Bi:Cu=1:1) thin films as precursor resulted in the CuI impurity in $CuBiI_4$ (The corresponding XRD results are illustrated in Supplementary information as Fig. S1).

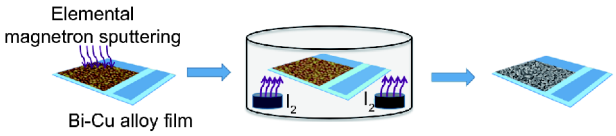

Figure 1 Schematics of the preparation of copper bismuth iodide.

Since there are few standard PDF card related to the $CuBiI_4$ crystal structure, we need to carefully deal with XRD data. Fig. 2 shows the XRD results of the prepared samples using Bi-Cu alloy thin films as precursors. Diffraction peaks can be indexed well with the reference data [42], and the peaks labeled with diamond symbols come from the ITO substrate. All the matched XRD peaks indicate $CuBiI_4$ films with cubic structure. About 0.03° of 2θ shifts of the diffraction peaks may be ascribed to the internal horizontal strains of the thin-film induced by the different thermal expansion coefficients [36]. For these samples based on Bi-Cu alloy, the high-index as well as low-index planes in [111] direction with 2θ at 12.72° and 25.50° corresponded to (111) plane and (222) plane, respectively. And the (440) plane with weak intensity at 42.23° is also included.

UPS, UV-vis and photolumescence (PL) measurements were carried out to analyze the energy band structure of $CuBiI_4$ materials. UPS results determine the valence band energy level of the prepared samples (Fig. 3a and b). The work function can be determined by the difference value between the photon energy and the binding energy of the secondary cutoff edge from the equation E_F=Source Energy (He I)$-E_{cutoff}$, where, the energy of monochromatic light (He I source) is 21.2 eV, and the secondary

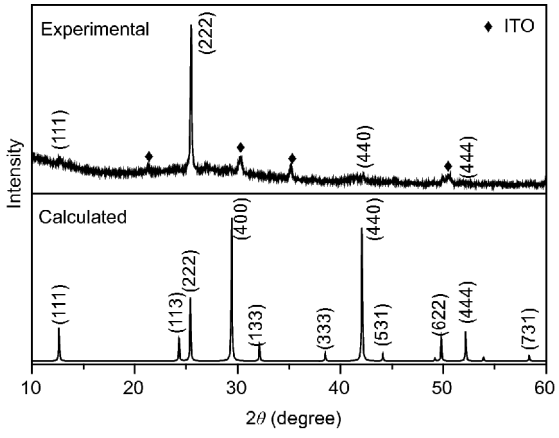

Figure 2 XRD pattern of the as-prepared copper bismuth iodide $CuBiI_4$ based on Bi-Cu alloy (Dataset ID sd_1123303 from springer materials database used as calculated XRD [42]).

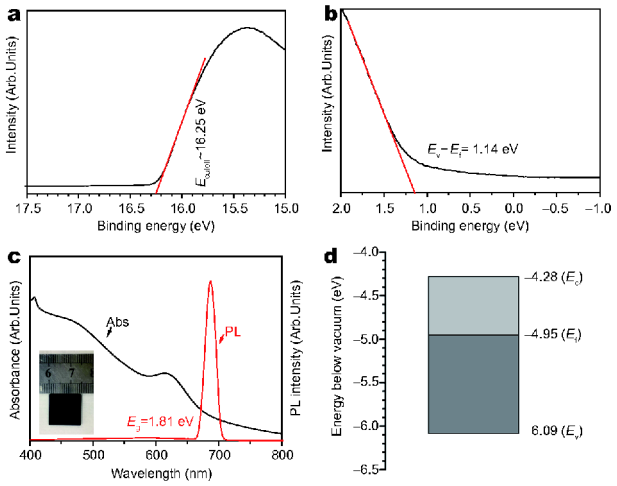

Figure 3 UPS measurements (a, b), UV–Vis and PL (226 nm light excited) results (c) and experimental band energy level (d) of the resulting $CuBiI_4$ thin films.

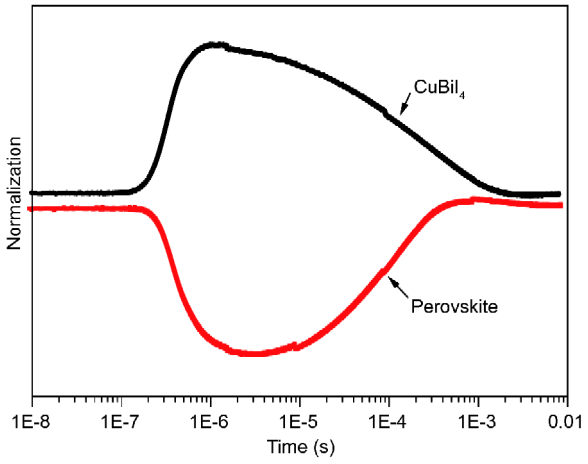

Figure 4 TPV results of the $CuBiI_4$ thin film based on Bi-Cu alloy and a classical $CH_3NH_3PbI_3$ thin film sample prepared by a standard one-step solution method.

cutoff edge is 16.25 eV. The energy of E_F was calculated to be 4.95 eV [33,34]. The linear extrapolation in low binding-energy region indicates the value of (E_V−E_F), leading to an E_V of 6.09 eV. A broad light absorption region has been recorded in the $CuBiI_4$ thin film from UV to visible zone. Bandgap of the prepared $CuBiI_4$ was measured and calculated from the UV-vis spectra to be about 1.81 eV, which is also confirmed by the strong PL peak at 685 nm (Fig. 3c). Consequently, the conduction band (E_C) energy of the prepared $CuBiI_4$ material was calculated to be 4.28 eV. The corresponding energy level is illustrated in Fig. 3d. It can be found that the E_F energy level is above the middle of the bandgap, which indicates the obtained $CuBiI_4$ compound may be an n-type semiconductor. It is very interesting to note that our band-gap (1.81 eV) is quite different from that obtained by Hayase's group (2.67 eV) due to the different reaction conditions. Further research on the reaction and crystal growth is needed to clarify such a band gap difference.

Transient photovoltage (TPV) measurements were conducted under a 355 nm light with about 8 μJ power to evaluate the photoinduced charge carrier dissociation, transfer and recombination in $CuBiI_4$ thin films (Fig. 4). A classical $CH_3NH_3PbI_3$ thin film prepared by solution method was used as control. For the $CH_3NH_3PbI_3$ thin film, a negative TPV signal means that it is a p-type semiconductor [43] due to the accumulation of photoinduced electrons at the surface. The recombination time of photoinduced electrons is about 6×10^{-4} s. Completely different from the TPV result of $CH_3NH_3PbI_3$, a positive signal observed from the $CuBiI_4$ thin film suggested that the $CuBiI_4$ material is an n-type semiconductor [44,45], which is in good agreement with the UPS result. Importantly, the recombination time of the $CuBiI_4$ thin film is about 1×10^{-3} s, which signifies an even longer life time of photoinduced charge carrier of $CuBiI_4$ than that of $CH_3NH_3PbI_3$. These comparisons with $CH_3NH_3PbI_3$ lead halide perovskite material suggested that the current $CuBiI_4$ (lead-free perovskite-like material) can be a promising candidate for future photovoltaic device.

Fig. 5a illustrates the cross-section of the $CuBiI_4$ thin film on ITO surface. The total thickness of $CuBiI_4$ thin film is about 300 nm. By comparison, the related SEM image of cross-section of Bi-Cu alloy thin film is listed in Fig. S2b, and the thickness is about ~80 nm. HRTEM measurements of the crystalline $CuBiI_4$ were carried out on a thinner $CuBiI_4$ thin film, which was *in-situ* fabricated on the surface of Mo grid by the same DMSER method. The lattices of the $CuBiI_4$ crystalline are very clear, the average distance of which is 3.51 Å. These lattices can be well indexed with the plane of (222) (Fig. 5b). Based on the $CuBiI_4$ thin film on ITO substrate, solar cell devices were assembled and the SEM image of the cross-section is shown in Fig. 5c. The related EDS measurements can be found in Fig. S3. Interestingly, there is a very dense, pinhole-free and uniform cross-section appearance in the device compared with the pristine porous $CuBiI_4$ thin film. It can be attributed to the dissolution of polar solvent of 4-*tert*-butyl pyridine (TBP), acetonitrile, and infiltration of organic Spiro-MeOTAD in the re-

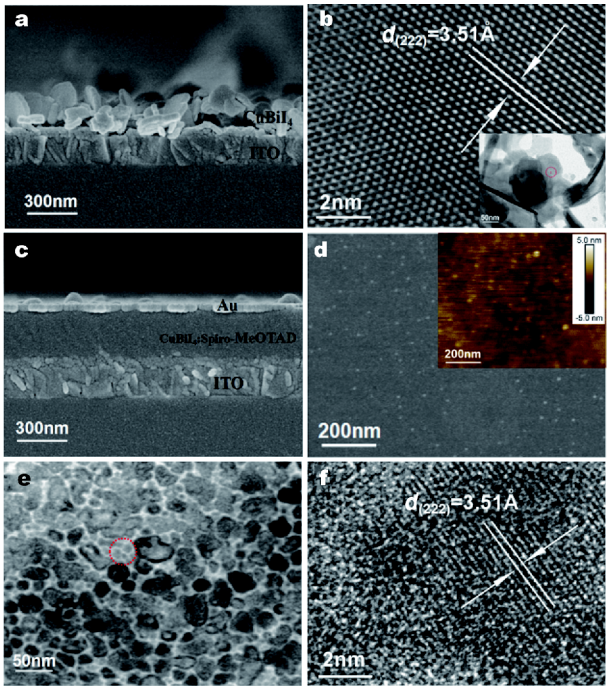

Figure 5 Cross-section of the as-prepared $CuBiI_4$ thin film on ITO surface (a); HRTEM image of the crystalline $CuBiI_4$ (b); cross-section of the solar cell device with ITO/$CuBiI_4$:Spiro-MeOTAD/Au (c); surface morphology of the compact bulk heterojunction $CuBiI_4$:Spiro-MeOTAD (Inset is the AFM result of $CuBiI_4$:Spiro-MeOTAD surface. The corresponding AFM result of Bi-Cu alloy thin film is illustrated in supporting information as Fig. S2a) (d); TEM image of the bulk heterojunction $CuBiI_4$:Spiro-MeOTAD thin film (e); HRTEM of crystalline $CuBiI_4$ in $CuBiI_4$:Spiro-MeOTAD inorganic organic hybrid bulk thin film (f).

crystallized $CuBiI_4$ structures. We believed that the pristine $CuBiI_4$ thin film can be recrystallized in such a mixed solution with polar organic solvent during the spin-coating process. The surface morphology of the $CuBiI_4$:Spiro-MeOTAD hybrid thin film was also characterized by SEM (Fig. 5d) and AFM. With the mixed solvents of TBP and acetonitrile assisted spin-coating, a uniform surface could be obtained. By comparison, the related surface SEM image of pristine $CuBiI_4$ has been illustrated in Fig. S4. For further understanding the structure of $CuBiI_4$:Spiro-MeOTAD hybrid thin film, TEM and HRTEM measurements were carried out. Fig. 5e and f show the TEM and HRTEM images of $CuBiI_4$:Spiro-MeOTAD, respectively. We could clearly see that the crystalline $CuBiI_4$ domains are surrounded by organic Spiro-MeOTAD (with low contrast) to form a $CuBiI_4$:Spiro-MeOTAD hybrid bulk-heterojunction structure (Fig. 5e). The average lattice distance in the inorganic part is still 3.51 Å, which confirms that no decomposition happened in the crystalline $CuBiI_4$ after the re-crystallization. This novel bulk-heterojunction structure may facilitate the photoinduced charge carrier separation and transfer in the perovskite-like solar cells. To clarify the advantages of this bulk-heterojunction structure, PL and TPV measurements of the $CuBiI_4$:Spiro-MeOTAD thin films were carried out. The TPV signal was enhanced (Fig. S5a) while PL intensity was significantly decreased in the $CuBiI_4$:Spiro-MeOTAD thin films (Fig. S5b). These results confirmed that the $CuBiI_4$:Spiro-MeOTAD bulk-heterojunction could separate and transfer the photo-induced charge carrier more efficiently than the bare $CuBiI_4$ material.

Fig. 6a shows the schematic of the $CuBiI_4$:Spiro-MeOTAD hybrid solar cell device. The $CuBiI_4$ thin films were *in situ* fabricated on an ITO substrate without any electron transfer materials (e.g., TiO_2, ZnO), $CuBiI_4$:Spiro-MeOTAD hybrid bulk layer is between the ITO and Au electrodes that form a sandwich structure to generate and separate photoinduced charge carriers. The corresponding band energy level alignment is plotted as Fig. 6b, where the gray black $CuBiI_4$ thin film is the main absorber to generate non-equilibrium photo-induced carrier. The photo-generated electrons are transferred to the ITO, and the holes are collected by the Au electrode through the Spiro-MeOTAD. Photoelectric conversion efficiency (PCE) of $CuBiI_4$:Spiro-MeOTAD hybrid solar cell devices was evaluated by a solar light simulator (0.69 suns) equipped with Xe light and AM 1.5G filter. We have optimized the device fabrication process by adjusting the thickness of the pristine $CuBiI_4$ and the best PCE of the champion device is 1.119% with a 0.375 V of open circuit voltage (V_{OC}), 7.184 mA cm^{-2} of short circuit current density (J_{SC}) and 28.673% of fill factor (FF) based on ~110 nm alloy precursor thin films. Till now, it is the highest record for $CuBiI_4$ based solar cells. For the solar cell samples using 80 nm alloy precursor, a 0.479 V of V_{OC}, 2.621 mA cm^{-2} of J_{SC}, 36.629% of FF and 0.692% of PCE have obtained. The corresponding external quantum efficiency (EQE) curve of the solar cell device is shown in Fig. 6d. The band gap of $CuBiI_4$, calculated from EQE, is about 1.79 eV, which further confirmed the UV-vis and PL results. It demonstrates that the current $CuBiI_4$ prepared by Bi-Cu alloy possesses a broad photoelectric response. In this work, the PCE of the fabricated solar cell devices are not high. The small FF of solar cell devices indicate that the recombination of photogenerated charge carriers is serious, so further optimization of the solar cell devices is still needed. We believe that the $CuBiI_4$ is a promising candidate material for future lead free solar energy harvesting device application.

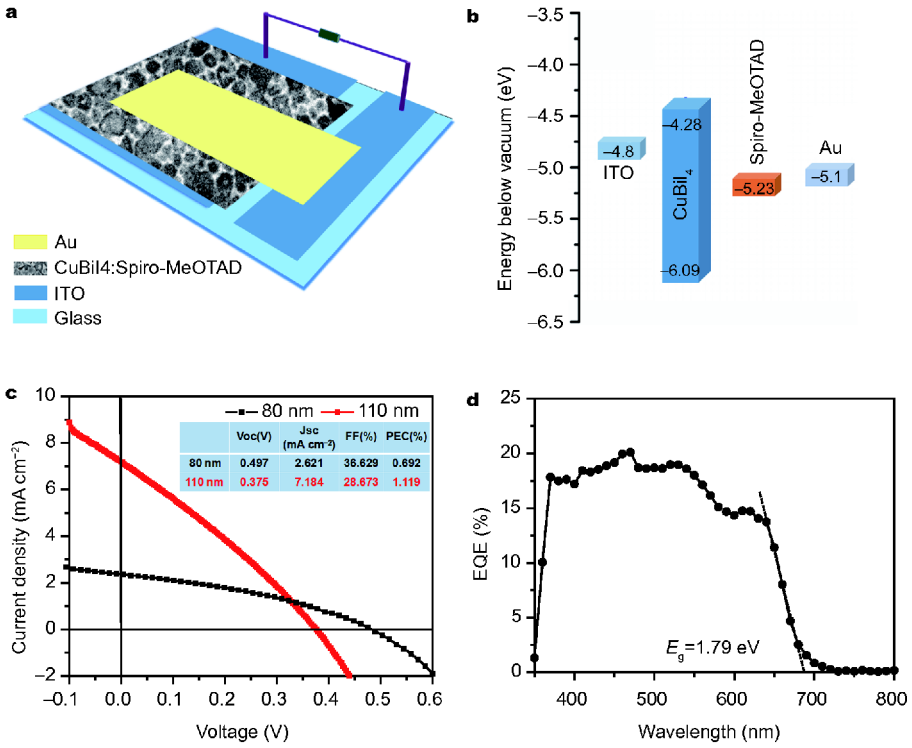

Figure 6 Schematic of the $CuBiI_4$:Spiro-MeOTAD hybrid solar cell device (a); band energy level alignment of the materials (b); *J*−*V* curve of the $CuBiI_4$:Spiro-MeOTAD hybrid solar cell device (c); EQE curve of the $CuBiI_4$:Spiro-MeOTAD hybrid solar cell device (d).

CONCLUSION

In this work, (222) plane oriented $CuBiI_4$ perovskite-like semiconductor thin films were successfully fabricated by the *in-situ* reaction of Bi-Cu alloy with I_2 at room temperature without using any organic solvent. The band structure of this material was preliminarily studied by UPS, UV-vis and PL. Energy level of top of valence band and bottom energy level of conduction band are calculated to be −6.09 and −4.28 eV. Further, the carrier type of resulting $CuBiI_4$ material was measured as an n-type semiconductor by TPV analysis. Importantly, the $CuBiI_4$ material also shows a promising photoelectric characteristic comparable to a $CH_3NH_3PbI_3$ thin film through measuring the photoinduced charge carrier dynamic of the materials. The surface morphology of the $CuBiI_4$ thin films become very uniform, compact, and pinhole-free after the spin-coating of Spiro-MeOTAD with mixed organic solvent due to the influence of TBP and acetonitrile. The recrystallization of flake-like $CuBiI_4$ and the formation of a $CuBiI_4$:Spiro-MeOTAD bulk heterojunction structure was accomplished at the same time. Based on this hybrid structure, a PCE of 1.119% have been obtained, which is the highest record of $CuBiI_4$ based solar cell device till now. Our current reaction design based on Bi-Cu alloy, formation of dense bulk-heterojunction film, as well as the sandwich solar cell device configuration, may open a new way for future all-inorganic lead-free perovskite-like $A_aB_bX_x$ photovoltaic.

Received 28 July 2018; accepted 9 September 2018; published online 12 October 2018

1 Kojima A, Teshima K, Shirai Y, *et al.* Organometal halide perovskites as visible-light sensitizers for photovoltaic cells. J Am Chem Soc, 2009, 131: 6050–6051
2 Molina-Ontoria A, Zimmermann I, Garcia-Benito I, *et al.* Benzotrithiophene-based hole-transporting materials for 18.2% perovskite solar cells. Angew Chem Int Ed, 2016, 55: 6270–6274
3 Burschka J, Pellet N, Moon SJ, *et al.* Sequential deposition as a route to high-performance perovskite-sensitized solar cells. Nature, 2013, 499: 316–319
4 Chen H, Ye F, Tang W, *et al.* A solvent- and vacuum-free route to large-area perovskite films for efficient solar modules. Nature, 2017, 131: 92–95
5 Zhou H, Chen Q, Li G, *et al.* Interface engineering of highly efficient perovskite solar cells. Science, 2014, 345: 542–546
6 Yang WS, Park BW, Jung EH, *et al.* Iodide management in formamidinium-lead-halide–based perovskite layers for efficient solar cells. Science, 2017, 356: 1376–1379
7 Zhang C, Gao L, Hayase S, *et al.* Current advancements in material

research and techniques focusing on lead-free perovskite solar cells. Chem Lett, 2017, 46: 1276–1284
8 Shi Z, Guo J, Chen Y, *et al.* Lead-free organic-inorganic hybrid perovskites for photovoltaic applications: recent advances and perspectives. Adv Mater, 2017, 29: 1605005
9 Hoefler SF, Trimmel G, Rath T. Progress on lead-free metal halide perovskites for photovoltaic applications: a review. Monatsh Chem, 2017, 148: 795–826
10 Hao F, Stoumpos CC, Cao DH, *et al.* Lead-free solid-state organic–inorganic halide perovskite solar cells. Nat Photonics, 2014, 8: 489–494
11 Xi J, Wu Z, Jiao B, *et al.* Multichannel interdiffusion driven $FASnI_3$ film formation using aqueous hybrid salt/polymer solutions toward flexible lead-free perovskite solar cells. Adv Mater, 2017, 29: 1606964
12 Noel NK, Stranks SD, Abate A, *et al.* Lead-free organic–inorganic tin halide perovskites for photovoltaic applications. Energy Environ Sci, 2014, 7: 3061–3068
13 Zhu Z, Chueh CC, Li N, *et al.* Realizing efficient lead-free formamidinium tin triiodide perovskite solar cells *via* a sequential deposition route. Adv Mater, 2018, 30: 1703800
14 Cheng P, Wu T, Zhang J, *et al.* $(C_6H_5C_2H_4NH_3)_2GeI_4$: A layered two-dimensional perovskite with potential for photovoltaic applications. J Phys Chem Lett, 2017, 8: 4402–4406
15 Stoumpos CC, Frazer L, Clark DJ, *et al.* Hybrid germanium iodide perovskite semiconductors: active lone pairs, structural distortions, direct and indirect energy gaps, and strong nonlinear optical properties. J Am Chem Soc, 2015, 137: 6804–6819
16 Konstantakou M, Stergiopoulos T. A critical review on tin halide perovskite solar cells. J Mater Chem A, 2017, 5: 11518–11549
17 Zhang X, Wu G, Gu Z, *et al.* Active-layer evolution and efficiency improvement of $(CH_3NH_3)_3Bi_2I_9$-based solar cell on TiO_2-deposited ITO substrate. Nano Res, 2016, 9: 2921–2930
18 Ma Z, Peng S, Wu Y, *et al.* Air-stable layered bismuth-based perovskite-like materials: Structures and semiconductor properties. Physica B-Condensed Matter, 2017, 526: 136–142
19 Chen X, Myung Y, Thind A, *et al.* Atmospheric pressure chemical vapor deposition of methylammonium bismuth iodide thin films. J Mater Chem A, 2017, 5: 24728–24739
20 Vigneshwaran M, Ohta T, Iikubo S, *et al.* Facile synthesis and characterization of sulfur doped low bandgap bismuth based perovskites by soluble precursor route. Chem Mater, 2016, 28: 6436–6440
21 Singh T, Kulkarni A, Ikegami M, *et al.* Effect of electron transporting layer on bismuth-based lead-free perovskite $(CH_3NH_3)_3Bi_2I_9$ for photovoltaic applications. ACS Appl Mater Interfaces, 2016, 8: 14542–14547
22 Zhang Z, Li X, Xia X, *et al.* High-quality $(CH_3NH_3)_3Bi_2I_9$ film-based solar cells: pushing efficiency up to 1.64%. J Phys Chem Lett, 2017, 8: 4300–4307
23 Lehner AJ, Fabini DH, Evans HA, *et al.* Crystal and electronic structures of complex bismuth iodides $A_3Bi_2I_9$ (A=K, Rb, Cs) related to perovskite: aiding the rational design of photovoltaics. Chem Mater, 2015, 27: 7137–7148
24 Park BW, Philippe B, Zhang X, *et al.* Bismuth based hybrid perovskites $A_3Bi_2I_9$ (A: methylammonium or cesium) for solar cell application. Adv Mater, 2016, 27: 6806–6813
25 Johansson MB, Zhu H, Johansson EMJ. Extended photo-conversion spectrum in low-toxic bismuth halide perovskite solar cells. J Phys Chem Lett, 2016, 7: 3467–3471
26 Bai F, Hu Y, Hu Y, *et al.* Lead-free, air-stable ultrathin $Cs_3Bi_2I_9$ perovskite nanosheets for solar cells. Sol Energy Mater Sol Cells, 2018, 184: 15–21
27 Pazoki M, Johansson MB, Zhu H, *et al.* Bismuth iodide perovskite materials for solar cell applications: Electronic structure, optical transitions, and directional charge transport. J Phys Chem C, 2016, 120: 29039–29046
28 Greul E, Petrus ML, Binek A, *et al.* Highly stable, phase pure $Cs_2AgBiBr_6$ double perovskite thin films for optoelectronic applications. J Mater Chem A, 2017, 5: 19972–19981
29 Yang B, Chen J, Yang S, *et al.* Lead-free silver-bismuth halide double perovskite nanocrystals. Angew Chem Int Ed, 2018, 57: 5359–5363
30 McClure ET, Ball MR, Windl W, *et al.* Cs_2AgBiX_6 (X = Br, Cl): new visible light absorbing, lead-free halide perovskite semiconductors. Chem Mater, 2016, 28: 1348–1354
31 Savory CN, Walsh A, Scanlon DO. Can Pb-free halide double perovskites support high-efficiency solar cells? ACS Energy Lett, 2016, 1: 949–955
32 Turkevych I, Kazaoui S, Ito E, *et al.* Photovoltaic rudorffites: Lead-free silver bismuth halides alternative to hybrid lead halide perovskites. ChemSusChem, 2017, 10: 3754–3759
33 Jung KW, Sohn MR, Lee HM, *et al.* Silver bismuth iodides in various compositions as potential Pb-free light absorbers for hybrid solar cells. Sustain Energy Fuels, 2018, 2: 294–302
34 Kim Y, Yang Z, Jain A, *et al.* Pure cubic-phase hybrid iodobismuthates $AgBi_2I_7$ for thin-film photovoltaics. Angew Chem Int Ed, 2016, 55: 9586–9590
35 Fourcroy HP, Carré D, Thévet F, *et al.* Structure du tétraiodure de cuivre(I) et de bismuth(III), $CuBiI_4$. Acta Crystallogr C, 1991, 47: 2023-2025
36 Hu Z, Wang Z, Kapil G, *et al.* Solution-processed air-stable copper bismuth iodide for photovoltaics. ChemSusChem, 2018, 11: 2930–2935
37 Zhang L, Lei Y, Yang X, *et al.* A facile room temperature iodination route to *in situ* fabrication of patterned copper-iodide/silicon quasi-bulk-heterojunction thin films for photovoltaic application. Dalton Trans, 2015, 44: 5848–5853
38 Lei Y, Yang X, Gu L, *et al.* Room-temperature preparation of tri-silver-copper-sulfide/polymer based heterojunction thin film for solar cell application. J Power Sources, 2015, 280: 313–319
39 Lei Y, Jia H, He W, *et al.* Hybrid solar cells with outstanding short-circuit currents based on a room temperature soft-chemical strategy: the case of P_3HT:Ag_2S. J Am Chem Soc, 2012, 134: 17392–17395
40 He Y, Lei Y, Yang X, *et al.* Using elemental Pb surface as a precursor to fabricate large area $CH_3NH_3PbI_3$ perovskite solar cells. Appl Surf Sci, 2016, 389: 540–546
41 Lei Y, Gu L, Yang X, *et al.* Fast chemical vapor-solid reaction for synthesizing organometal halide perovskite array thin films for photodetector applications. J Alloys Compd, 2018, 766: 933–940
42 https://materials.springer.com/isp/crystallographic/docs/sd_1123303
43 Lei Y, Gu L, He W, *et al.* Intrinsic charge carrier dynamics and device stability of perovskite/ZnO mesostructured solar cells in moisture. J Mater Chem A, 2016, 4: 5474–5481
44 Yang X, Liu R, Lei Y, *et al.* Dual influence of reduction annealing on diffused hematite/FTO junction for enhanced photoelectrochemical water oxidation. ACS Appl Mater Interfaces, 2016, 8: 16476–16485

45 Jing L, Zhou W, Tian G, *et al.* Surface tuning for oxide-based nanomaterials as efficient photocatalysts. Chem Soc Rev, 2013, 42: 9509–9549

Acknowledgements This work was supported by the National Natural Science Foundation of China (21673200, 61504117 and U1604121), the Innovation Scientists and Technicians Troop Construction Projects of Henan Province (144200510014).

Author contributions Zhang B did the experiments and collected the related data. Lei Y analyzed the data and prepared the manuscript. Qi R measured the TEM and HRTEM of the samples. Yu H carried out the TPV experiments of the samples. Yang X revised the manuscript. Cai T analyzed the XRD results. Zheng Z directed the whole project.

Conflict of interest The authors declare no conflict of interest.

Supplementary Information Supplementary data are available in the online version of the paper.

Busheng Zhang is currently pursuing his Master degree at the North China University of Water Resources and Electric Power. His research is focused on the thin film solar cells.

Zhi Zheng is currently a professor at Xuchang University. He received his PhD degree from the Chemistry Department of Chinese University of Hong Kong in 2003. His current research interest includes organic-inorganic hybrid thin film solar cells and perovskite solar cells.

室温原位法制备$CuBiI_4$材料及其在体相异质结太阳能电池中的应用

张卜生[1,2], 雷岩[1*], 齐瑞娟[3], 余海丽[1], 杨晓刚[1], 蔡拓[1], 郑直[1*]

摘要 铋和铜作为无毒且储量相对丰富的金属元素，都非常适合新型无铅卤化物钙钛矿材料及相应光伏器件的设计和制备. 本文采用非常简单的气-固反应方法，以铋铜合金作为前驱体直接在ITO基底上室温原位制备了一种新型铜铋碘($CuBiI_4$)化合物薄膜材料. XRD和TEM的测试结果证实了这种具有(222)优势晶面取向$CuBiI_4$晶体薄膜的生成. 瞬态表面光电压(TPV)测试表明我们制备的$CuBiI_4$是一种n型半导体材料，且具有与$CH_3NH_3PbI_3$钙钛矿材料相当的光生载流子分离与传输性能. UV-Vis, PL和IPCE等结果表明灰黑色$CuBiI_4$的禁带宽度大约为1.81 eV, 适合作为光伏材料. 值得注意的是，我们利用四叔丁基吡啶(TBP)、乙腈和Spiro-MeOTAD有机混和溶剂旋涂处理后，得到了一种混合均匀、致密、平滑的$CuBiI_4$:Spiro-MeOTAD本体异质结薄膜. 基于这种新型薄膜，我们制备了具有简单三明治结构的ITO/$CuBiI_4$:Spiro-MeOTAD/Au杂化太阳能电池器件，并获得了1.119%的光电转化效率. 这种室温下金属表面元素直接反应的方法(DMSER)为未来无铅钙钛矿或类钙钛矿化合物($A_aB_bX_x$)的制备及其在高性能光伏器件中的应用提供了一个全新的策略.

